

The influence of grains on the propagation and structure of C-type shock waves in interstellar molecular clouds

D. R. Flower¹★ and G. Pineau des Forêts^{2,3}

¹Physics Department, The University, Durham DH1 3LE

²IAS, Université de Paris-Sud, F-92405 Orsay, France

³LUTH, Observatoire de Paris, F-92195 Meudon Cedex, France

Accepted 2003 April 1. Received 2003 March 31; in original form 2003 March 14

ABSTRACT

Gas–grain interactions can have important consequences for the physics and chemistry of shock waves propagating in molecular clouds. The grains can be both a source and a sink of molecules, and their inertia can modify the dynamics of the propagation of, in particular, C-type shock waves. The degree of charging of the grains, both in the pre-shock gas and in the shock wave itself, is a significant parameter. The population of interstellar grains extends from large molecules, which we represent by polycyclic aromatic hydrocarbons, to much larger particles, composed of silicates and amorphous carbon material. The influence of the inertia of the grains on the dynamics of the flow is modelled in detail, and upper limits to the velocities of C-type shock waves are established. We find that collisions between charged and neutral grains, driven by ion–neutral drift in C-type shock waves, may lead to the shattering of a large fraction of the amorphous carbon material.

Key words: atomic processes – MHD – molecular processes – shock waves – ISM: clouds – dust, extinction.

1 INTRODUCTION

Grains of various sizes and compositions are a component of the interstellar medium. The term ‘grains’ is sometimes understood as encompassing both large molecules, such as polycyclic aromatic hydrocarbons (PAHs), and bulk materials such as graphite or silicates. Mathis, Rumpl & Nordsieck (1977) deduced a grain size distribution, of the diffuse interstellar medium in the solar vicinity, of the form $dn_g(a)/da \propto a^{-3.5}$, where $dn_g(a)$ is the number density of grains in the interval of radius from a to $a + da$. It follows from this distribution that small grains are the most numerous, whereas large grains incorporate most of the mass.

Our aim in the present paper is to establish the influence that grains may have on the structure, even the existence of continuous (C-type) shock waves. In weakly ionized media, charged grains can affect the dynamics in two ways: they enhance the momentum transfer from the neutral to the ionized fluid; they increase the inertia of the ionized fluid and hence affect the magnetosonic speed. Neutral grains, on the other hand, are usually considered to be of little consequence for the dynamics, as their mass density is small compared with that of the neutral gas.

Draine & Sutin (1987) concluded that, under the conditions relevant to dark molecular clouds, most grains are negatively and singly charged. More recently, Weingartner & Draine (2001a) showed that small carbonaceous grains ($a < 15 \text{ \AA}$) are predominantly uncharged in the ‘cold, neutral medium’. The charging of grains is determined

by the rates of attachment of electrons and ions and the rates of electron detachment by the ultraviolet radiation field. In the interiors of ‘dark’ clouds, the gas and dust are shielded from the general interstellar radiation field by external dust. However, cosmic rays give rise to secondary electrons, of which the energy is approximately 30 eV (Cravens & Dalgarno 1978). These secondary electrons collisionally excite electronic states of H_2 , giving rise to ultraviolet fluorescence (Prasad & Tarafdar 1983; Gredel, Lepp & Dalgarno 1987; Sternberg, Dalgarno & Lepp 1987). The fluorescence photons, which have energies of around 10 eV, can dissociate and ionize molecules and atoms in the gas phase; they can also detach electrons from grains.

In Section 2, we specify the rate coefficients that we have adopted to determine the charge of both small and large grains within the interiors of dark molecular clouds. The results of calculations of the equilibrium charge distribution of the grains are presented in Section 3; these pre-shock conditions are then adopted (in Section 4) when computing models of C-type shock waves propagating in the medium. We make our concluding remarks in Section 5.

2 THE ELECTRICAL CHARGING OF GRAINS IN DARK CLOUDS

2.1 Small grains (large carbonaceous molecules)

Pineau des Forêts, Flower & Dalgarno (1988) and Weingartner & Draine (2001a) have considered the reactions that lead to the electrical charging of PAH. In both studies, extensive use was made

★E-mail: david.flower@durham.ac.uk

of the work of Omont (1986). Here we specify the rate coefficients that we have adopted for reactions involving PAH molecules, taking $C_{54}H_{18}$ as representative. According to Omont (1986, equation 2), the radius of the corresponding palette is $a = 6.6 \text{ \AA}$.

2.1.1 Electron attachment to PAH

In the environment of dark clouds, PAH are predominantly neutral or singly charged. Electrons interact with neutral PAH through a polarization potential and with charged PAH through the Coulomb potential. For electron attachment to neutral PAH,



we adopt $k_1 = 1.8 \times 10^{-6} s_e \text{ cm}^3 \text{ s}^{-1}$, where s_e is the electron sticking probability. Weingartner & Draine (2001a, fig. 6) compiled measurements of the sticking probability from various sources. There is an order of magnitude spread in the values measured for molecules containing a number of carbon atoms N_C between 60 and 70 ($0.01 \leq s_e \leq 0.1$); we adopt $k_1 = 1.0 \times 10^{-7} \text{ cm}^3 \text{ s}^{-1}$, corresponding to $s_e = 0.06$. In the high-temperature gas within a C-type shock wave, it may be more appropriate to adopt the geometrical cross-section of the PAH and the mean thermal speed of the electrons when evaluating the rate coefficient of reaction (1). For $T_e = 10^4 \text{ K}$ and $s_e = 0.06$, this approach yields $k_1 = 5.1 \times 10^{-8} \text{ cm}^3 \text{ s}^{-1}$, which is within a factor of 2 of the value adopted and well within the uncertainty in s_e .

For the recombination of electrons with PAH^+ ,



we take $k_2 = 3.3 \times 10^{-6} (300/T_e)^{1/2} \text{ cm}^3 \text{ s}^{-1}$. This expression derives from the work of Omont (1986) and assumes an electron sticking probability $s_e = 0.3$. Weingartner & Draine (2001a, fig. 7) compiled measurements of s_e for $N_C \leq 14$. The experimental data show considerable scatter and appear to suggest that s_e decreases with increasing N_C , whereas their fit predicts the opposite trend. The value that we have adopted, $s_e = 0.3$, is consistent with the fit of Weingartner & Draine (2001a), to within the uncertainties involved.

2.1.2 Electron detachment by the radiation field

The general interstellar ultraviolet radiation field does not penetrate into the interiors of dark clouds, owing to absorption by dust in the external layers. Cosmic rays, on the other hand, do penetrate the interiors of the clouds and ionize the gas. The ‘secondary’ electrons produced by cosmic ray ionization of hydrogen, the most abundant element, have sufficient energy to collisionally excite Rydberg electronic states of H_2 , which then fluoresce in the ultraviolet, emitting photons with energies $7.1 < h\nu < 14.6 \text{ eV}$. Denoting the rate of cosmic ray ionization of hydrogen per unit volume by ζn_H , where $n_H = n(H) + 2n(H_2)$, the number of fluorescence photons generated per unit volume and time is $0.15\zeta n_H$; 0.15 is the fraction of the secondary electrons that collisionally excite the Rydberg states of H_2 .

Consider now the photoionization of PAH molecules by the fluorescence photons. Omont (1986) estimated the photoionization cross-section of PAH^0 as $\sigma = 3 \times 10^{-2} a^2 = 1.3 \times 10^{-16} \text{ cm}^2$ for the case of $N_C = 54$. The geometric cross-section is πa^2 , and hence the ionization probability is approximately 10^{-2} . Most of the ultraviolet fluorescence photons are absorbed by larger grains, for which we adopt the grain size distribution $dn_g(a)/da \propto a^{-3.5}$ of Mathis et al. (1977). With a range of grain radii $0.01 \leq a \leq 0.3 \mu\text{m}$ and a total grain mass density of $0.0119 n_H m_H$ (see Section 2.2 below), where m_H is the mass of the hydrogen atom, we obtain $\langle n_g \sigma \rangle = 7.1 \times 10^{-11} n_H$

cm^{-3} for the mean grain number density and $\langle n_g \sigma \rangle = 9.1 \times 10^{-22} n_H \text{ cm}^{-1}$ for the mean grain opacity. The geometric cross-section of a spherical grain of radius a has been assumed; real grains may, of course, have a more complex geometrical structure. The fraction of the fluorescence photons that ionize the representative PAH^0 (with $N_C = 54$) is determined by the ratio of the corresponding opacities, $1.3 \times 10^{-16} n(PAH^0) / (9.1 \times 10^{-22} n_H) = 1.4 \times 10^5 [n(PAH^0) / n_H]$.

The rate of photoionization of PAH^0 ,



is obtained from the ratio of opacities and the number of fluorescence photons generated per unit volume and time ($0.15\zeta n_H$), yielding $2 \times 10^4 \zeta n(PAH^0) \text{ cm}^{-3} \text{ s}^{-1}$. For the photodetachment of electrons from PAH^- ,



we adopt the analogous expression, $2 \times 10^4 \zeta n(PAH^-) \text{ cm}^{-3} \text{ s}^{-1}$. When $n_{PAH}/n_H = 10^{-6}$, which corresponds to approximately 15 per cent of the available carbon ($n_C/n_H = 3.55 \times 10^{-4}$; see Table 1) being in the form of PAH, a fraction 0.13 of the fluorescence photons is absorbed by PAH molecules and the remainder by larger grains.

2.1.3 Reactions with positive ions

PAH^- and positive (atomic and molecular) ions X^+ interact through the Coulomb potential and can mutually neutralize:



Following Omont (1986), we take $k_5 = 7.5 \times 10^{-8} (300/T_e)^{1/2} \text{ cm}^3 \text{ s}^{-1}$ for the reaction with H^+ , where a reaction probability of 0.3 per collision is assumed. The rate coefficients for reactions with heavier ions, which include PAH^+ , were obtained by dividing by $M_i^{1/2}$, where M_i is the ion mass in amu.

Ions are likely to undergo charge transfer with PAH^0 , which has a low ionization potential ($\approx 7 \text{ eV}$):



The interaction between the PAH^0 and the positive ion is mediated by the polarization potential. Adopting a reaction probability per collision of 0.1, we obtain $k_6 = 4.4 \times 10^{-9} \text{ cm}^3 \text{ s}^{-1}$ for the reaction with H^+ . Once again, the rate coefficients for reactions with heavier ions were reduced by $M_i^{1/2}$.

The reaction probability for charge transfer (reaction 6) was taken to be smaller than the value of 0.3 for mutual neutralization (reaction 5). The electron affinity of a PAH is less than its first ionization potential, but its proton affinity is large, comparable to its ionization potential (Omont 1986). It follows that the rate coefficient for proton attachment to PAH^0 may exceed the value that we have adopted for k_6 . However, protons are not the most abundant ions in dark clouds.

2.1.4 Electron detachment by neutrals

Neutral species may possibly react with PAH^- , detaching the electron, as in



We include representative reactions with H, C, CH and OH, as well as with O. The rate coefficient was taken to be $3.0 \times 10^{-9} \exp(-E_a/kT)$ for the reaction with H and smaller by $M^{1/2}$ for heavier neutral species; these reactions may have an activation energy, $E_a \leq 1 \text{ eV}$. If so, their rates are negligible in cold gas, but the reactions become important in C-type shock waves, owing to the ion–neutral velocity difference (Pineau des Forêts et al. 1988).

Table 1. Fractional elemental abundances, n_X/n_H , and their adopted distribution across the phases of the medium; this compilation is based upon the studies of Anders & Grevesse (1989), Savage & Sembach (1996), Gibb et al. (2000) and Sofia & Meyer (2001). The fractional abundance of the PAH is $n_{\text{PAH}}/n_H = 1.0 \times 10^{-6}$. Numbers in parentheses are powers of 10.

Element	Fractional abundance	Gas phase	PAH	Grain mantles	Grain cores
H	1.00	1.00			
He	1.00 (−1)	1.00 (−1)			
C	3.55 (−4)	8.27 (−5)	5.40 (−5)	5.53 (−5)	1.63 (−4)
N	7.94 (−5)	6.39 (−5)		1.55 (−5)	
O	4.42 (−4)	1.24 (−4)		1.78 (−4)	1.40 (−4)
Mg	3.70 (−5)				3.70 (−5)
Si	3.37 (−5)				3.37 (−5)
S	1.86 (−5)	1.47 (−5)		3.93 (−6)	
Fe	3.23 (−5)	1.50 (−8)			3.23 (−5)

2.2 Large grains

The ‘large’ grains are assumed to be bulk carbonaceous material or silicates, with a size distribution $dn_g(a)/da \propto a^{-3.5}$ (Mathis et al. 1977) in the range of radii $0.01 \leq a \leq 0.3 \mu\text{m}$; the distribution was assumed to be the same for the neutral and for the charged grains. The total mass density of the grains (including their mantles) is $0.0119n_H m_H$ (see Section 3 below), where m_H is the mass of the hydrogen atom.

We note that other size distributions are possible (cf. Weingartner & Draine 2001b), which may be more appropriate to dark clouds; but the distribution of Mathis et al. (1977) provides a point of reference for future investigations of the phenomena being considered here.

2.2.1 Electron attachment

The rate of electron attachment to neutral grains is $n_e(n_{g0}/n_g)n_g\sigma v_e s_e$, where $v_e = (8kT_e/\pi m_e)^{1/2}$ is the mean thermal speed of the electrons, n_e is the electron number density, n_{g0} is the density of neutral grains and n_g is the total grain density. With $\langle n_g\sigma \rangle = 9.1 \times 10^{-22}n_H \text{cm}^{-1}$ and $s_e = 0.5$ (Weingartner & Draine 2001a, equation 28), we obtain a rate per unit volume of

$$n_e n_H (n_{g0}/n_g) 4.9 \times 10^{-15} (T_e/300)^{1/2} \text{cm}^{-3} \text{s}^{-1},$$

corresponding to a rate coefficient of $6.9 \times 10^{-5} (T_e/300)^{1/2} \text{cm}^3 \text{s}^{-1}$.

If the cross-section for electron attachment is assumed to be determined by the polarization of the neutral grain by the electron, a situation which may obtain for small grains at low collision energies, then the ‘Langevin’ value of the rate coefficient is $2\pi(e^2\alpha/m_e)^{1/2}$, where α is the polarizability of the grain. We take $\alpha = a^3$, where a is the grain radius (Omont 1986; Draine & Sutin 1987). The Langevin model identifies an ‘orbiting’ radius for the colliding particle (here, an electron), which is a position of unstable equilibrium. The electron has equal probability of moving in towards the grain or of moving out to infinity (in which case, there is no reaction). Thus, the maximum value of the rate coefficient for attachment is $\pi(e^2\alpha/m_e)^{1/2}$. Following Weingartner & Draine (2001a), we assume that an impacting electron has a maximum probability $s_e = 0.5$ of sticking to the grain (rather than being elastically scattered). Then, taking $a = 0.01 \mu\text{m}$, corresponding to the lower limit of the adopted size distribution, we obtain a rate coefficient of $2.5 \times 10^{-5} \text{cm}^3 \text{s}^{-1}$ by applying the Langevin method; this may be compared with $1.8 \times 10^{-5} \text{cm}^3 \text{s}^{-1}$ when the mean geometric cross-section of the grains is adopted and at $T_e = 20 \text{K}$. Thus, the assumption of a polarization interaction leads to a rate coefficient for electron attachment to a

neutral grain of radius $a = 0.01 \mu\text{m}$, which is approximately 40 per cent larger than the mean value that we have adopted (at $T_e = 20 \text{K}$).

The rate of electron attachment to positively charged grains is proportional to their fractional abundance, (n_{g+}/n_g) , but is enhanced by the attractive long-range Coulomb potential at low collision velocities (low temperatures). Le Bourlot et al. (1995) derived, from the analysis of Draine & Sutin (1987), an approximate expression for the enhancement factor, which, for the grain size distribution adopted here, is $(1 + 450/T_e)$. The rate per unit volume of the neutralization of positively charged grains by electrons is then

$$n_e n_H (n_{g+}/n_g) 4.9 \times 10^{-15} (T_e/300)^{1/2} (1 + 450/T_e) \text{cm}^{-3} \text{s}^{-1},$$

where, once again, we have adopted $s_e = 0.5$ (Weingartner & Draine 2001a, equation 30).

2.2.2 Electron detachment by the radiation field

The rate of detachment of electrons from grains by the fluorescence photons is $0.15\zeta n_H f y \text{cm}^{-3} \text{s}^{-1}$, where ζ is the rate (s^{-1}) of cosmic ray ionization of hydrogen, f is the fraction of the fluorescence photons that is absorbed by the grains and y is the detachment probability. The value of f depends on the fractional abundance of PAH. When $n_{\text{PAH}}/n_H = 10^{-6}$, a fraction 0.13 of the fluorescence photons is absorbed by the PAH (see Section 2.1.2) and hence $f = 0.87$, whereas $f = 0.99$ when $n_{\text{PAH}}/n_H = 10^{-7}$.

Weingartner & Draine (2001a, fig. 5) plotted the photoelectric yields, y , of silicate and carbonaceous grains, for a range of sizes and also for the bulk materials. At a photon energy $h\nu = 10 \text{eV}$, near the centre and the maximum of the spectrum of the fluorescence photons (cf. Gredel 1990), the yield is approximately 0.03 for neutral, bulk carbonaceous material and almost twice this value for neutral, bulk silicate; the asymptotic values of these yields, for $h\nu \geq 15 \text{eV}$, are approximately 0.2 and 0.08, respectively. The accurate evaluation of the rate of photoionization by the fluorescence photons requires the convolution of the spectrum of fluorescence photons and the photoelectric yield, for a range of grain sizes. This is a non-trivial task, which is probably not justified at present in view of the uncertainties in the values of the yields and the limited importance of positively charged grains in molecular clouds. Accordingly, we adopt $y = 0.03$ for electron detachment from neutral grains.

There is considerable uncertainty in the probability of photodetachment of an electron from negatively charged grains. In his discussion of photodetachment (from PAH^-), Omont (1986) proposed adopting, for the detachment probability, the value of the probability of photoionization (of PAH^0) at comparable energies above threshold. Recalling that the threshold for photodetachment is smaller than for photoionization, this proposal would suggest the adoption of the asymptotic values of the photoelectric yields of the neutral grains as the photodetachment probabilities of negatively charged grains, i.e. $y = 0.2$ for bulk carbonaceous material and $y = 0.08$ for silicate.

An alternative method of estimating y for negatively charged grains is offered by the analysis of Weingartner & Draine (2001a, equation 19), who fitted the photodetachment cross-section of C_6F_6^- , as measured by Christophorou, Datskos & Faidas (1994). Weingartner & Draine expressed the cross-section as being proportional to the oscillator strength for photodetachment, f_{pdt} , and they adopted $f_{\text{pdt}} = 0.5$ in their fit to the measurements. The oscillator strength f_{pdt} is the probability that photon absorption occurs into the continuum, resulting in electron detachment. This probability varies with energy above threshold and, at the maximum in

the cross-section (which, in the notation of Weingartner & Draine, occurs at $x = 1$), is equal to 0.3.

In the calculations reported below, we adopted $y = 0.2$ as an estimate of the probability of photodetachment of electrons from the negative grains by the fluorescence photons.

2.2.3 Attachment of positive ions

Neutral grains can acquire charge by attachment of positive ions. The rate of attachment per unit volume is derived by analogy with the corresponding expression in Section 2.2.1 as

$$n_i n_H (n_{g0}/n_g) 4.9 \times 10^{-15} (m_e/m_i)^{1/2} (T_i/300)^{1/2} \text{ cm}^{-3} \text{ s}^{-1},$$

where n_i is the density, T_i is the temperature and m_i is the mass of the ion and m_e is the mass of the electron.

2.2.4 Neutralization by positive ions

Negatively charged grains can be neutralized by collisions with positive ions. The rate of neutralization per unit volume is derived by analogy with the corresponding expression in Section 2.2.1 as

$$n_i n_H (n_{g-}/n_g) 4.9 \times 10^{-15} (m_e/m_i)^{1/2} \times (T_i/300)^{1/2} (1 + 450/T_i) \text{ cm}^{-3} \text{ s}^{-1},$$

where n_i is the density, T_i is the temperature and m_i is the mass of the ion and m_e is the mass of the electron.

The numerical values adopted for the reaction rate coefficients are summarized in Appendix A.

3 THE EQUILIBRIUM CHARGE DISTRIBUTION

Here we consider the grain charge distribution in equilibrium and then, in Section 4, the propagation of C-type shocks into the medium. The density of protons in the gas is $n_H \approx n(\text{H}) + 2n(\text{H}_2)$. The elemental abundances and their initial distribution across the phases of the medium (gas and solid) are shown in Table 1. We have assumed

that all of the Mg and Si, and most of the Fe, are in silicate grains, specifically olivine (MgFeSiO_4), and that observations of diffuse interstellar clouds (Savage & Sembach 1996) yield the fractions of the elements that are not bound in the grain cores. The elemental oxygen abundance, $n_{\text{O}}/n_{\text{H}} = 4.42 \times 10^{-4}$, is consistent with the recent determination of Sofia & Meyer (2001), based on observations of F and G stars. When the fractional abundance of the PAH is $n_{\text{PAH}}/n_{\text{H}} = 1.0 \times 10^{-6}$, as in Table 1, the contribution of PAH to the ‘grain’ mass density is $0.67 \times 10^{-3} n_{\text{H}} m_{\text{H}}$, which is an order of magnitude smaller than that ($7.8 \times 10^{-3} n_{\text{H}} m_{\text{H}}$) of the material of the grain cores, assumed to be carbonaceous or composed of silicates. The contribution of the mantles is $4.0 \times 10^{-3} n_{\text{H}} m_{\text{H}}$, giving a total ‘grain’ (including PAH) mass density of $12.6 \times 10^{-3} n_{\text{H}} m_{\text{H}}$ and hence, with $n_{\text{He}}/n_{\text{H}} = 0.10$, a grain:gas mass density ratio of $G = 9.0 \times 10^{-3}$. The adopted chemical composition of the grain mantles is shown in Table 2. We assume that the ratio of the abundances of solid CO, in the grain mantles, and of gas-phase CO is 0.10 and that 20 per cent of the elemental sulphur is present as H_2S in the grain mantles.

A fractional abundance of PAH $n_{\text{PAH}}/n_{\text{H}} = 1.0 \times 10^{-6}$ yields a fraction of carbon in PAH of 5.4×10^{-5} (cf. Table 1), which is consistent with the (still uncertain) estimates of the fraction of carbon in very small grains (Li & Draine 2001; Weingartner & Draine 2001a). We shall also consider lower values, $n_{\text{PAH}}/n_{\text{H}} = 1.0 \times 10^{-7}$ and 1.0×10^{-8} .

The gas-phase chemistry involved species containing the elements listed in Table 1 and comprised approximately 1000 reactions, including ion–neutral, neutral–neutral, charge transfer, radiative and dissociative recombination (see <http://ccp7.dur.ac.uk> and <http://aristote.biophy.jussieu.fr/MIS>). Photoreactions other than those induced by the H_2 fluorescence radiation were excluded.

Table 3 shows the charge distribution for PAH and larger grains, calculated for $n_{\text{PAH}}/n_{\text{H}} = 1.0 \times 10^{-6}$ and $n_{\text{PAH}}/n_{\text{H}} = 1.0 \times 10^{-7}$; the gas density is $n_{\text{H}} = 10^4 \text{ cm}^{-3}$. In the case of $n_{\text{PAH}}/n_{\text{H}} = 1.0 \times 10^{-6}$, and for a rate of cosmic ray ionization of hydrogen $\zeta = 5 \times 10^{-17}$

Table 2. Fractional abundances of the chemical species composing the grain mantles [based mainly on the study of W33A by Gibb et al. (2000)]. Numbers in parentheses are powers of 10.

CO	CO ₂	CH ₄	NH ₃	H ₂ O	CH ₃ OH	H ₂ CO	HCOOH	OCS	H ₂ S
8.3 (−6)	1.3 (−5)	1.6 (−6)	1.6 (−5)	1.0 (−4)	1.9 (−5)	6.2 (−6)	7.2 (−6)	2.1 (−7)	3.7 (−6)

Table 3. The fractional abundances of PAH molecules and larger grains, $n(\text{X})/n_{\text{H}}$, and of the electrons, n_e/n_{H} , calculated for a gas density $n_{\text{H}} = 10^4 \text{ cm}^{-3}$. In the case of $\zeta = 5 \times 10^{-17} \text{ s}^{-1}$ and a total fractional abundance of PAH $n_{\text{PAH}}/n_{\text{H}} = 1.0 \times 10^{-6}$, results are given both excluding and including the effects of electron detachment and ionization of PAH and larger grains by the H_2 ultraviolet fluorescence radiation field. The neutral fractions of PAH and of larger grains are also given. Numbers in parentheses are powers of 10.

$n_{\text{PAH}}/n_{\text{H}} =$	$\zeta = 5 \times 10^{-17} \text{ s}^{-1}$			$\zeta = 1 \times 10^{-17} \text{ s}^{-1}$	
	1.0×10^{-6} without fluorescence photons	1.0×10^{-6} with fluorescence photons	1.0×10^{-7} with fluorescence photons	1.0×10^{-6} with fluorescence photons	1.0×10^{-7} with fluorescence photons
PAH ⁰	8.68 (−07)	8.68 (−07)	5.44 (−08)	9.35 (−07)	7.07 (−08)
PAH ⁺	6.72 (−10)	1.23 (−09)	1.48 (−11)	1.18 (−09)	1.63 (−11)
PAH [−]	1.31 (−07)	1.31 (−07)	4.55 (−08)	6.35 (−08)	2.92 (−08)
PAH ⁰ /PAH	0.87	0.87	0.54	0.94	0.71
g ⁰	3.94 (−11)	6.13 (−11)	4.72 (−11)	6.41 (−11)	5.20 (−11)
g ⁺	8.70 (−14)	3.55 (−12)	5.94 (−13)	2.40 (−12)	4.15 (−13)
g [−]	3.15 (−11)	6.18 (−12)	2.31 (−11)	4.46 (−12)	1.86 (−11)
g ⁰ /g	0.56	0.86	0.67	0.90	0.73
e [−]	1.16 (−08)	1.17 (−08)	6.24 (−08)	2.68 (−09)	1.45 (−08)

s^{-1} , results are given both with and without including the effects of the H_2 fluorescence radiation field on the charge of the PAH.

With the exception of PAH^+ , which is a minor species, the results for PAH are independent of the fluorescence photon field. Our results are not directly comparable with those of Weingartner & Draine (2001a, fig. 9), who included the effects of the mean interstellar radiation field; but we note that these authors also predicted that PAH of radius $a = 7 \text{ \AA}$ are predominantly neutral in the ‘cold, neutral medium’. Table 3 also shows that, when $n_{PAH}/n_H = 1.0 \times 10^{-6}$, the PAH^- carry a large fraction of the total negative charge of the medium; in the case of $\zeta = 5 \times 10^{-17} \text{ s}^{-1}$, approximately 90 per cent of the electrons are attached to PAH molecules, thereby reducing the number available for attachment to larger grains.

The charge distribution of the larger grains, on the other hand, does depend on the rates of electron photodetachment by the fluorescence radiation field. Because the large grains absorb most of these fluorescence photons, the fractional abundance of positively charged grains is much higher, and that of negatively charged grains is lower, when electron detachment by the fluorescence photons is included. The fraction of the neutral grains decreases when the total fractional abundance of PAH is reduced to $n_{PAH}/n_H = 1.0 \times 10^{-7}$, because there are more free electrons available for attachment to the larger grains. In the case of the lower value of the cosmic ray ionization rate, $\zeta = 1 \times 10^{-17} \text{ s}^{-1}$, and for both values of the total fractional abundance of PAH, $n_{PAH}/n_H = 1.0 \times 10^{-6}$ and 1.0×10^{-7} , the preponderance of neutral over charged PAH and larger grains is enhanced, relative to the case of $\zeta = 5 \times 10^{-17} \text{ s}^{-1}$, owing to the reduction in the overall degree of ionization at the lower value of ζ . Even when the fractional abundance of PAH is reduced to $n_{PAH}/n_H = 1.0 \times 10^{-8}$, in which case $n(PAH^-) \ll n_e$, the fractions $n(PAH^0)/n_{PAH} = 0.49$ and $n_{g0}/n_g = 0.47$ remain large.

We conclude that, in the interiors of dark clouds, from which the general interstellar radiation field is excluded, a large fraction, perhaps most of the grains are uncharged.

4 C-TYPE SHOCK WAVES IN DARK MOLECULAR CLOUDS

4.1 The propagation of C-type shock waves

A necessary condition for a C-type shock wave to propagate in a medium is that the magnetosonic speed should exceed the shock speed. The magnetosonic speed (at zero temperature) is defined by $v_m^2 = B^2/(4\pi\rho_c)$,

(8)

where B is the magnetic induction, transverse to the flow and ρ_c is the mass density of the charged species, which interact with the magnetic field. The charged species are ions, electrons and charged grains, and the electrons may be neglected because of their relatively small mass. The charged large grains are particularly significant in this context because they are the main contributors to the mass density of the charged fluid. Furthermore, Ciolek & Mouschovias (1993) have argued that the neutral grains may in effect be coupled to the charged grains, owing to the rapidity of grain charge-changing reactions (cf. Section 2.2 above).

Let us consider the pre-shock gas. The neutral grains become charged through attachment reactions or through ionization by the fluorescence photon field at a net frequency

$$\begin{aligned} \tau_0^{-1} \equiv \tau_{<}^{-1} + \tau_{>}^{-1} &= n_e(n_H/n_g)4.9 \times 10^{-15} \\ &\times (T_e/300)^{1/2} + 0.15\zeta f y (n_H/n_g) \\ &+ n_i(n_H/n_g)4.9 \times 10^{-15} (m_e/m_i)^{1/2} (T_i/300)^{1/2} \text{ s}^{-1}, \end{aligned} \quad (9)$$

where f is the fraction of the fluorescence photons that is absorbed by the larger grains (as distinct from the PAH) and y is the photoionization probability (see Section 2.2 above); τ_0 is the mean time during which a grain remains neutral. $\tau_{<}^{-1}$ is the rate at which neutral grains become negatively charged, through electron attachment, whereas $\tau_{>}^{-1}$ is the rate at which neutral grains become positively charged, through photoionization and attachment of a positive ion.

Negative grains are neutralized through attachment of positive ions and electron detachment by the fluorescence photons. These two reactions neutralize the negative grains at a net frequency

$$\begin{aligned} \tau_{-}^{-1} &= n_i(n_H/n_g)4.9 \times 10^{-15} (m_e/m_i)^{1/2} (T_i/300)^{1/2} \\ &\times (1 + 450/T_i) + 0.15\zeta f y' (n_H/n_g) \text{ s}^{-1}, \end{aligned} \quad (10)$$

where y' is the photodetachment probability and τ_{-} is the mean time that a grain remains negatively charged. Finally, positive grains are neutralized by recombination with electrons at a frequency

$$\tau_{+}^{-1} = n_e(n_H/n_g)4.9 \times 10^{-15} (T_e/300)^{1/2} (1 + 450/T_e) \text{ s}^{-1}. \quad (11)$$

The cyclotron frequency of the charged grains around the magnetic field lines is

$$\tau_{g\pm}^{-1} = eB/(2\pi c m_{g\pm}), \quad (12)$$

where $e/c = 1.6 \times 10^{-20} \text{ emu}$ and B (G) is the magnetic field strength; $m_{g\pm}$ is the mass of the charged grain.

Consider the case $\tau_{g\pm}^{-1} \gg \tau_0^{-1}, \tau_{-}^{-1}, \tau_{+}^{-1}$, i.e. the gyrofrequency is large compared with the frequencies at which the charge of the grain fluctuates. Then, the grain charge distribution is effectively ‘frozen’, and the charged grains are well coupled to the lines of the magnetic field. At the other extreme, $\tau_{g\pm}^{-1} \ll \tau_0^{-1}, \tau_{-}^{-1}, \tau_{+}^{-1}$, the grains change from being neutral to being charged frequently in a single gyroperiod. Under these conditions, the fraction of the grains (charged and neutral), which may be considered to be attached to the field lines, depends on the fraction of the time for which, on average, a grain is charged. In charge equilibrium,

$$n_{g0}\tau_0^{-1} = n_{g-}\tau_{-}^{-1} + n_{g+}\tau_{+}^{-1} \quad (13a)$$

$$n_{g-}\tau_{-}^{-1} = n_{g0}\tau_{<}^{-1} \quad (13b)$$

$$n_{g+}\tau_{+}^{-1} = n_{g0}\tau_{>}^{-1}, \quad (13c)$$

and the average value of the fraction of the charge-changing cycle during which a grain is neutral is given by

$$\frac{\tau_0}{\tau_0 + \tau_{+}\tau_{>}^{-1}/\tau_0^{-1} + \tau_{-}\tau_{<}^{-1}/\tau_0^{-1}},$$

where $\tau_{>}^{-1}/\tau_0^{-1}$ and $\tau_{<}^{-1}/\tau_0^{-1}$ are the relative probabilities that a neutral grain subsequently becomes positively or negatively charged. Using equation (13), and noting that $\tau_0^{-1} = \tau_{<}^{-1} + \tau_{>}^{-1}$ (equation 9) and that the total grain density is $n_g = n_{g0} + n_{g+} + n_{g-}$, it is readily shown that the fraction of the charge-changing cycle during which the grain is neutral is n_{g0}/n_g . It follows that a grain is charged for a fraction of its charge-changing cycle which is equal to the fraction of the grains that is charged. Accordingly, we shall assume that only the charged grains are attached to the magnetic field lines and subsequently flow with the ions and the electrons. We note that the large grains rapidly become negatively charged in the shock wave, owing to the increasing rate of electron attachment to the neutral grains, and practically the entire population of large grains is soon attached to the magnetic field.

In practice, some fraction of the grains decouples from the magnetic field, owing to collisions with the (abundant) neutrals in the medium. A parameter that has been used to assess the significance

of these collisions is $\omega_{g\pm}\tau_s$, where $\omega_{g\pm} = 2\pi\tau_{g\pm}^{-1}$ is the angular cyclotron frequency of the grains and τ_s is the time required for a mass of neutral gas comparable with the mass of the grain to collide with the grain (see, for example, Pilipp, Hartquist & Havnes 1990). When $\omega_{g\pm}\tau_s \leq 1$, collisions with the neutrals are sufficiently frequent to decouple the grain from the magnetic field lines. The product $\omega_{g\pm}\tau_s$ may be written as

$$\omega_{g\pm}\tau_s = eB/(c(\sigma v)n_H m_H), \quad (14)$$

where σ is the collision cross-section and v is the collision speed; $n_H \approx n(\text{H}) + 2n(\text{H}_2)$ and m_H is the mass of the hydrogen atom. Taking ‘typical’ conditions for dark clouds ($n_H = 10^4 \text{ cm}^{-3}$, $B = 10^{-4} \text{ G}$), adopting $\sigma = \pi a^2$, the geometrical cross-section of a grain of radius a , and with $v = (8kT/\pi m_H)^{1/2}$, the mean thermal speed at temperature T ($T = 20 \text{ K}$ in the pre-shock gas), we deduce that $\omega_{g\pm}\tau_s \leq 1$ when $a \geq 0.22 \text{ }\mu\text{m}$. For the size distribution which we consider (Mathis et al. 1977), approximately 18 per cent of the mass of the grains is comprised between $a = 0.22$ and $0.30 \text{ }\mu\text{m}$, the upper limit of the size distribution. We conclude that not all of the charged grains are initially coupled to the magnetic field and, in so assuming, we tend to overestimate the mass of the grains that are attached to the magnetic field and hence to underestimate the magnetosonic speed (equation 8).

In Table 4 we give the values of the magnetosonic speed, v_m , calculated assuming that only the charged grains are coupled to the magnetic field lines. Results are given for ranges of values of the fractional abundance of PAH and of the pre-shock gas density; two values of the cosmic ray ionization rate are considered, $\zeta = 5 \times 10^{-17}$ and $1 \times 10^{-17} \text{ s}^{-1}$. From this table, we conclude that v_m increases as the number density of electrons available for attachment to (neutral) grains decreases, i.e. as n_H increases, n_{PAH}/n_H increases, or ζ decreases. Adopting the scaling of the magnetic field strength with the gas density, $B(\mu\text{G}) = [n_H (\text{cm}^{-3})]^{1/2}$, we deduce that the values of v_m in Table 4 should be increased by a factor 1.10 for $n_H = 10^4 \text{ cm}^{-3}$ and by 1.34 for $n_H = 10^5 \text{ cm}^{-3}$, owing to the decoupling of the charged grains from the magnetic field lines in collisions with the neutral gas (see above).

The values of the magnetosonic speed, computed for $\zeta = 1 \times 10^{-17}$ and $5 \times 10^{-17} \text{ s}^{-1}$, are plotted in Fig. 1, where the effects of correcting for collisional decoupling are shown by the broken curves; the ‘critical’ shock speed computed by Le Bourlot et al. (2002) is also plotted in this figure. The critical speed is attained when the degree of dissociation of H_2 , the principal coolant, is sufficient for a thermal runaway to take place; a sonic point ensues, and the shock becomes J-type (cf. Le Bourlot et al. 2002). It may be seen from Fig. 1 that, for $n_{\text{PAH}}/n_H = 1.0 \times 10^{-6}$ and densities $n_H > 10^4 \text{ cm}^{-3}$, the upper limit to the speed of a C-type shock wave is determined by the collisional dissociation of H_2 , whereas, for $n_H < 10^4 \text{ cm}^{-3}$ or $n_{\text{PAH}}/n_H < 10^{-6}$, it is determined by the magnetosonic speed in the pre-shock gas.

Table 4. The magnetosonic speed (km s^{-1}) in the pre-shock gas at equilibrium, for the specified values of the cosmic ray ionization rate, ζ , the total fractional abundance of PAH, n_{PAH}/n_H , and of the gas density, n_H . No correction has been applied for the collisional decoupling of the charged grains from the magnetic field lines: see the discussion in Section 4.1.

$n_{\text{PAH}}/n_H =$ $n_H (\text{cm}^{-3})$	$\zeta = 5 \times 10^{-17} \text{ s}^{-1}$			$\zeta = 1 \times 10^{-17} \text{ s}^{-1}$		
	1.0×10^{-6}	1.0×10^{-7}	1.0×10^{-8}	1.0×10^{-6}	1.0×10^{-7}	1.0×10^{-8}
10^5	68	40	28	76	44	28
10^4	53	35	27	63	39	27
10^3	47	38	26	53	38	30

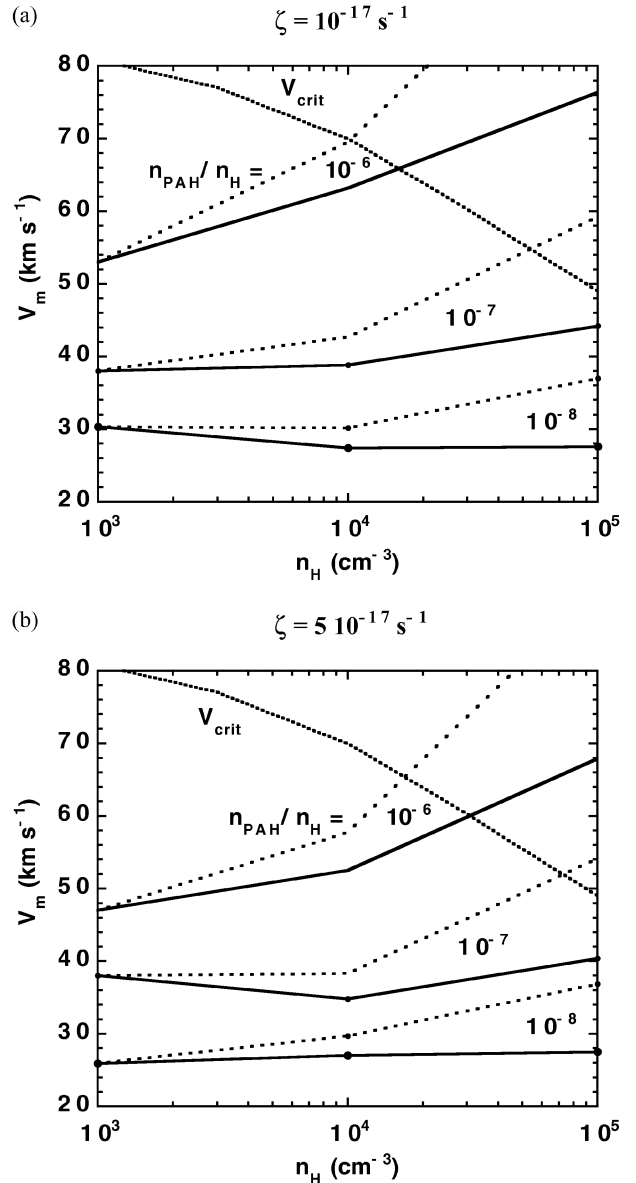


Figure 1. Values of the magnetosonic speed, v_m , computed for $10^3 < n_H < 10^5 \text{ cm}^{-3}$, $10^{-8} < n_{\text{PAH}}/n_H < 10^{-6}$, and (a) $\zeta = 1 \times 10^{-17} \text{ s}^{-1}$, (b) $\zeta = 5 \times 10^{-17} \text{ s}^{-1}$; the broken curves show the effects of correcting for collisional decoupling of the charged grains from the magnetic field lines (see the text, Section 4.1). The ‘critical’ velocity, v_{crit} , above which the shock becomes J-type (Le Bourlot et al. 2002) is also plotted (dotted line). This figure can be seen in colour in the on-line version of the journal on *Synergy*.

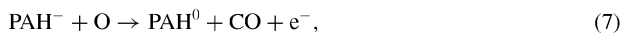
4.2 The structure of a C-type shock wave

We now consider an illustrative model of a planar, steady-state C-type shock wave. In Fig. 2 are plotted the velocity and temperature profiles computed through a shock wave of speed $v_s = 50$ km s^{-1} , pre-shock density $n_H \approx n(H) + 2n(H_2) = 10^4$ cm^{-3} and magnetic induction $B = 100$ μG ; the fractional abundance of PAH is $n_{PAH}/n_H = 1.0 \times 10^{-6}$ and the rate of cosmic ray ionization of hydrogen is $\zeta = 5 \times 10^{-17}$ s^{-1} . The independent variable is the flow time, $t = \int \frac{1}{v} dz$, of the neutral fluid, where z is the distance along the direction of flow. The initial value of the magnetosonic speed is $v_m = 53$ km s^{-1} ; see Table 4.

Of importance for the discussion below are the thermal and temperature profiles of the neutral and charged fluids. The ion–neutral drift that occurs in C-type shock waves, owing to the difference between the flow velocities of the charged and neutral particles, affects the rates of a variety of chemical and physical processes, not least that of grain shattering (see Section 4.3). We have considered in detail the processes that determine the dynamical structure of such shock waves (Le Bourlot et al. 2002) and believe that the code which we have used in the present work may be qualified as ‘state of the art’.

The temperature of the positive ions, T_i , initially increases to values of the order of 10^5 K as a consequence of the decreases in their flow speed, v_i (referred to the shock frame, in which $v_i = v_s = v_n$ initially), and kinetic energy. The rise in the temperature of the negatively charged fluid, T_e , is restricted by its thermal coupling to the neutral fluid. Following their initial rise, T_i and T_e respond to the chemical removal of ions and electrons through dissociative recombination, following ion–neutral reactions. The fractional abundance of the ions first increases, as v_i falls, and then decreases, as v_n falls and n_n rises, ultimately tending to its post-shock equilibrium value.

The charge variations of the large and small grains are quite different (see Fig. 3). The large grains become negatively charged as the electron temperature, and hence the rate of electron attachment, rises. On the other hand, the small grains (PAH) remain neutral, as electrons are detached from PAH^- in collisions with neutrals, e.g. in the reaction



for which we assumed an activation energy of 0.5 eV. The value of the activation energy is practically irrelevant, in so far as it is unlikely to exceed a few eV, whereas the kinetic energy of the O atom, associated with its flow relative to the PAH^- ion, attains about 200 eV. At such high impact energies, not only are the mantles of the (charged) grains removed completely by sputtering, but also significant erosion of the refractory cores of silicate and graphite grains occurs (cf. May et al. 2000).

The chemistry within the shock wave is complex. Significant fractions of the Fe and Si, which are initially bound in the cores of silicate grains (cf. Table 1), are eroded from charged grains by neutral particle impact in the shock wave, as may be seen in Fig. 4. Most of the positive charge is transferred to iron, through charge exchange reactions (cf. Fig. 5). Fig. 4 also shows that appreciable dissociation of H_2 to H occurs, owing to collisions of hydrogen molecules with drifting ions and electrons.

4.3 Collisions between charged and neutral grains

Collisions between grains might contribute to their disruption, releasing components of smaller size. This problem has been studied extensively by Jones et al. (1994) and Jones, Tielens & Hollenbach

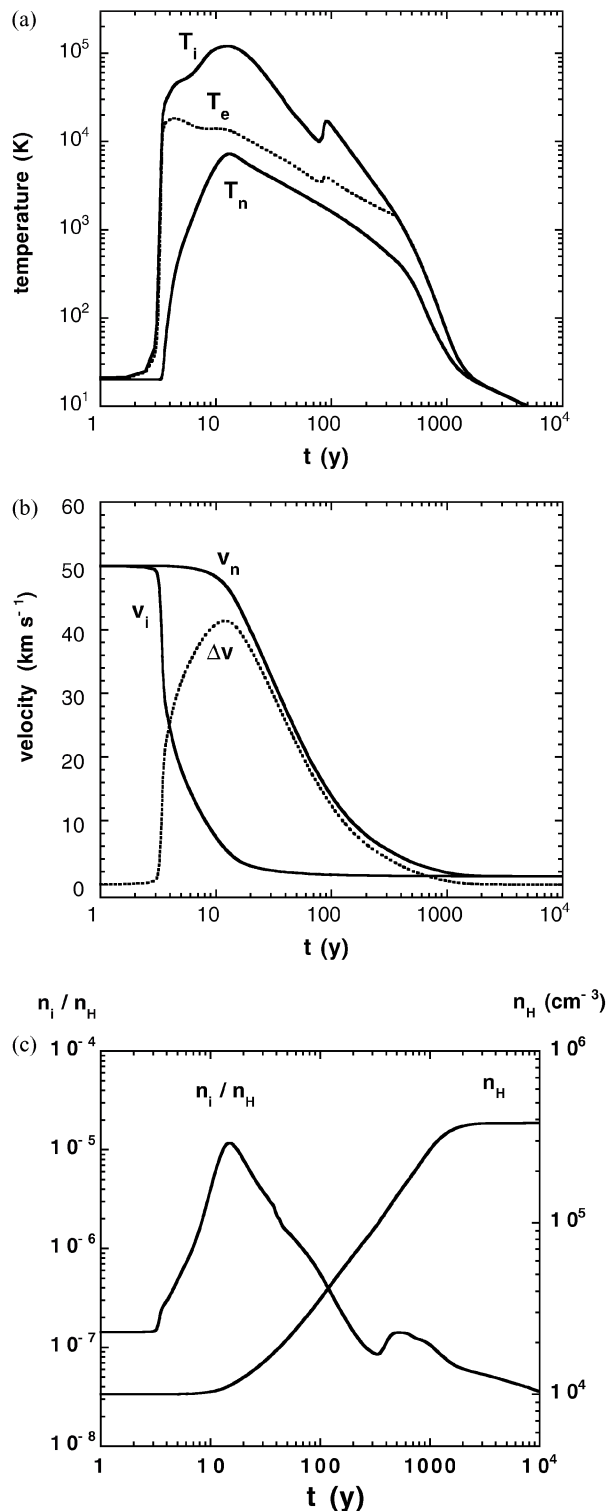


Figure 2. The profiles of (a) temperature, (b) velocity ($\Delta v = v_n - v_i$) and (c) fractional ionization and total gas density through a C-type shock wave of speed $v_s = 50$ km s^{-1} , pre-shock density $n_H \approx n(H) + 2n(H_2) = 10^4$ cm^{-3} and magnetic induction $B = 100$ μG ; the fractional abundance of PAH $n_{PAH}/n_H = 1.0 \times 10^{-6}$ and the rate of cosmic ray ionization of hydrogen is $\zeta = 5 \times 10^{-17}$ s^{-1} . The independent variable, t , is the flow time of the neutral fluid. This figure can be seen in colour in the on-line version of the journal on *Synergy*.

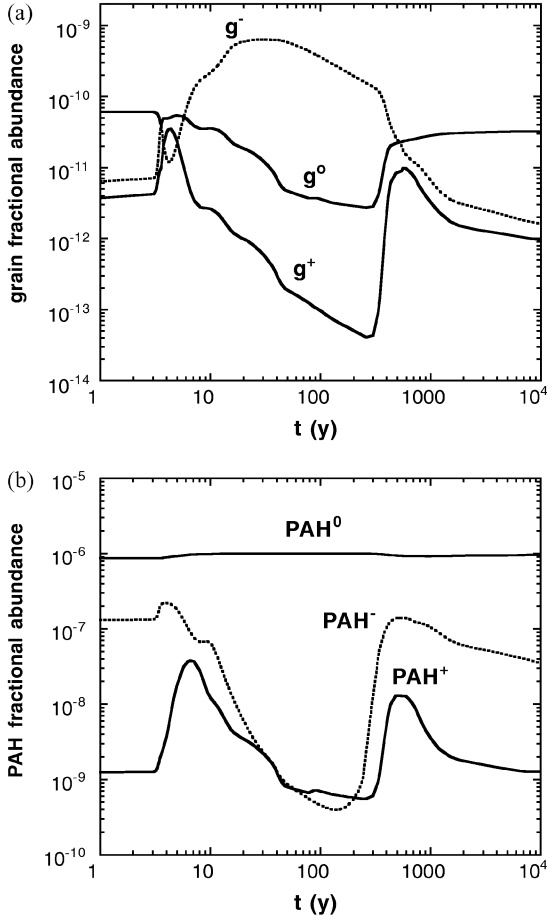


Figure 3. The variation of the fractional abundances of the neutral and charged forms of (a) the large grains ('g') and (b) the small grains ('PAH'); the model is the same as in Fig. 2. This figure can be seen in colour in the on-line version of the journal on *Synergy*.

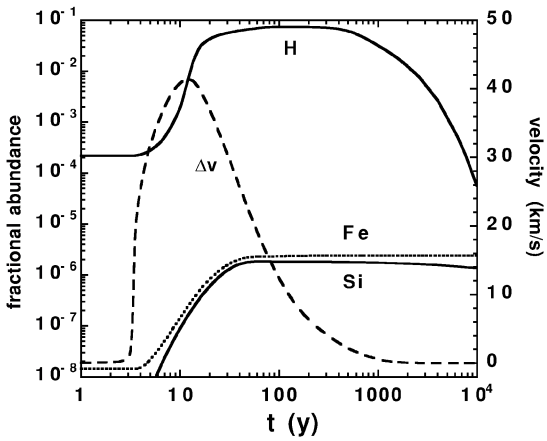


Figure 4. Illustrating the collisional dissociation of H_2 to H and the release of Fe and Si from silicate grains into the gas phase; the model is the same as in Fig. 2. The ion–neutral velocity difference, $\Delta v = v_n - v_i$, is also plotted. This figure can be seen in colour in the on-line version of the journal on *Synergy*.

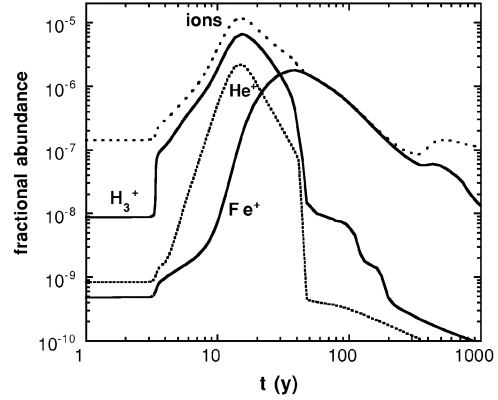


Figure 5. The fractional abundances of all and of the specified positive ions through the shock wave illustrated in Fig. 4; the transfer of positive charge to iron is evident. This figure can be seen in colour in the on-line version of the journal on *Synergy*.

(1996), in the context of grain shattering and destruction in J-type shock waves. Previously, Draine, Roberge & Dalgarno (1983) had suggested that grain–grain collisions might be an important destruction mechanism in C-type shock waves, owing to the relative motion of the charged and neutral fluids. Caselli, Hartquist & Havnes (1997) studied the sputtering of grains through collisions between small and large grains in C-type shock waves. Here, we consider the importance of shattering, in collisions between charged and neutral grains of comparable mass. We focus our attention on carbonaceous grains, for which the shattering may yield PAH (Omont 1986) and possible carriers of the diffuse interstellar bands.

Jones, Duley & Williams (1990) presented a model of interstellar grains of the amorphous carbon type. Such grains would contain single, double and triple carbon bond structures, with bond energies of 3.64, 7.26 and 9.88 eV, respectively (D. A. Williams, 2003, personal communication). In a collision between a charged and a neutral grain, each with the same number of carbon atoms, N_C , the relative kinetic energy associated with the ion–neutral drift is $\mu_g(v_n - v_i)^2/2$, where $\mu_g = N_C m_C/2$ is the reduced mass. The energy required to break a number n_s of single bonds is $n_s E_B = (n_s/N_C)N_C E_B$, where $E_B \approx 3.6$ eV. It follows that a relative collision speed of 7.5 km s^{-1} is sufficient to disrupt a number of single bonds $n_s = N_C/2$, causing major damage to the grain (shattering). One of the outcomes of the shattering would be the release into the gas phase of polyynes and large PAH molecules, as well as smaller atomic and molecular hydrocarbon fragments (Jones et al. 1990). It is the plausibility of this process that we now consider, in the context of C-type shocks in dark molecular clouds.

Jones et al. (1996) discussed at length the shattering of grains in grain–grain collisions. They defined ‘catastrophic destruction’ of a grain as occurring when ‘half the target grain is shocked to the tensile strength’. In their table 1, they listed values of the corresponding collision velocity, v_{cat} , for various grain materials and for the case of a projectile of radius $a_p = 50 \text{ \AA}$ impacting a target of radius $a_T = 1000 \text{ \AA}$ (0.1 \mu m). In the case of graphite/amorphous carbon grains, they obtained $v_{\text{cat}} = 75 \text{ km s}^{-1}$. Their fig. 5 shows that v_{cat} decreases as the dimension of the projectile increases towards that of the target. The critical velocities that they computed for $a_T = 1000 \text{ \AA}$ and $a_p = 100$ and 250 \AA may be reproduced approximately by scaling the value ($v_{\text{cat}} = 75 \text{ km s}^{-1}$) for $a_T = 1000 \text{ \AA}$ and $a_p = 50 \text{ \AA}$ on assuming that the centre-of-mass kinetic energy, $m_P m_T v_{\text{cat}}^2/[2(m_P + m_T)]$, remains constant. This

procedure yields $v_{\text{cat}} = 27 \text{ km s}^{-1}$ for $a_p = 100 \text{ \AA}$ and $v_{\text{cat}} = 7 \text{ km s}^{-1}$ for $a_p = 250 \text{ \AA}$, compared with 23 and 5 km s^{-1} , respectively, from fig. 5 of Jones et al. (1996). Using this same scaling, we obtain a critical velocity of only 1 km s^{-1} when the projectile and target have the same size ($a_p = a_T = 1000 \text{ \AA}$). We conclude that the criterion adopted above for major damage in a collision between large grains of the same size, which yields a threshold impact velocity of 7.5 km s^{-1} , probably overestimates the relative kinetic energy that is required.

In order to assess the possible significance of this process, we consider collisions between a charged grain and a neutral grain of the same radius, a . The frequency of this collision process is (cf. Le Boulot et al. 1995)

$$v = |v_n - v_i| \int \pi(2a)^2 dn_{g_0}(a) \text{ (s}^{-1}\text{)}, \quad (15)$$

where n_{g_0} is the number density of the neutral grains. We shall assume that all the grains, both charged and neutral, have the same size distribution and approximate equation (15) by

$$v = 4n_{g_0} \frac{\langle n_g \sigma \rangle}{\langle n_g \rangle} |v_n - v_i|, \quad (16)$$

where $\langle n_g \sigma \rangle = 9.1 \times 10^{-22} n_{\text{H}} \text{ cm}^{-1}$ is the mean opacity and $\langle n_g \rangle = 7.1 \times 10^{-11} n_{\text{H}} \text{ cm}^{-3}$ is the mean density; $|v_n - v_i|$ is the ion–neutral drift speed. The rate of such collisions between charged and neutral grains is $(n_{g^+} + n_{g^-})v \text{ cm}^{-3} \text{ s}^{-1}$. Regarding the threshold velocity for catastrophic destruction to occur, we make the assumption that $v_{\text{cat}} = 3 \text{ km s}^{-1}$ and probably underestimate the degree of shattering.

Fig. 6 illustrates the extent of the shattering of amorphous carbon grains in the case of the above model of a C-type shock wave. It may be seen that the ion–neutral velocity difference remains sufficiently large (in excess of 3 km s^{-1}) for long enough (a time comparable to the inverse of the grain–grain collision frequency) to cause shattering of more than half of the grains. The shattering process can remain effective in C-type shock waves of lower velocity. For example, when $v_s = 20 \text{ km s}^{-1}$, the ion–neutral velocity difference attains 14 km s^{-1} . Even when $v_s = 10 \text{ km s}^{-1}$, the velocity difference peaks at over 5 km s^{-1} . Indeed, the fraction of grains shattered at $v_s = 20 \text{ km s}^{-1}$ is somewhat larger than at the higher shock speed of $v_s =$

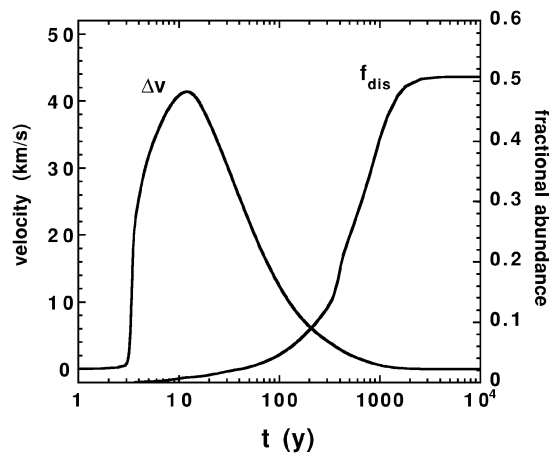


Figure 6. Illustrating shattering in collisions between the neutral and charged forms of amorphous carbon grains for the same model as in Fig. 4; f_{dis} is the fraction of the grains disrupted by this process. The ion–neutral velocity difference, $\Delta v = v_n - v_i$, is also plotted. This figure can be seen in colour in the on-line version of the journal on *Synergy*.

50 km s^{-1} . One reason is that the rate of charged grain–neutral grain collisions increases in proportion to n_{g_0} when g^0 is the minority grain species; in the case of the lower velocity shock, the fraction of neutral grains is larger. On the basis of these illustrative calculations, we conclude that collisions between amorphous carbon grains in C-type shock waves can lead to fragmentation of a substantial fraction, perhaps most of the grains.

5 CONCLUDING REMARKS

We have considered the interactions involving grains in dark molecular clouds, both in equilibrium and when perturbed by a shock wave. Small grains were represented by PAH molecules and large grains by silicates (specifically olivine, MgFeSiO_4) and amorphous carbon. The charge distribution of the grains was computed in the pre-shock gas, allowing not only for grain–gas interactions but also for the effects of the internal ultraviolet radiation field, which is produced subsequent to the ionization of hydrogen by cosmic rays (Prasad & Tarafdar 1983). The radiation field, which arises from fluorescence following electron collisional excitation of H_2 , has only a marginal effect on the charge distribution of the PAH molecules but a significant effect on that of the large grains. Both the PAH and the large grains are predominantly neutral in the medium at equilibrium.

The propagation of a shock wave into a medium of density $n_{\text{H}} = 10^4 \text{ cm}^{-3}$ and transverse magnetic induction $B = 100 \text{ \mu G}$ was studied. From considerations of the frequencies of grain charge-changing collisions, we concluded that only the charged grains are effectively coupled to the magnetic field. The steady-state structure of a shock wave of velocity $v_s = 50 \text{ km s}^{-1}$ was computed. As $v_s = 50 < v_m = 53 \text{ km s}^{-1}$, where v_m is the magnetosonic speed, the shock wave is of C-type. Whilst the small grains (PAH) are neutralized in the shock wave, through electron detachment reactions with neutrals, the large grains become predominantly negatively charged, owing to the attachment of electrons. Collisions between charged and neutral grains of amorphous carbon, at the ion–neutral drift velocity, are sufficiently energetic and frequent to lead to the shattering of more than half of these grains. This result confirms an early suggestion of Draine et al. (1983) that grain–grain collisions in C-type shock waves might be an important grain disruption mechanism. We plan a more detailed study of this process, involving the characterization and explicit treatment of grains of various sizes.

ACKNOWLEDGMENTS

We are indebted to David Williams for his (unpublished) review at a meeting on ‘The Diffuse Interstellar Bands’, organized by the Astrophysical Chemistry Group of the RSC and RAS in 2003 January at the University of Manchester Institute of Science and Technology. We are also grateful to the referee for a prompt and useful report on our submission.

REFERENCES

- Anders E., Grevesse N., 1989, *Geochim. Cosmochim. Acta*, 53, 197
 Caselli P., Hartquist T.W., Havnes O., 1997, *A&A*, 322, 296
 Christophorou L.G., Datskos P.G., Faidas H., 1994, *J. Chem. Phys.*, 101, 6728
 Ciolek G.E., Mouschovias T.C., 1993, *ApJ*, 418, 774
 Cravens T.E., Dalgarno A., 1978, *ApJ*, 219, 750
 Draine B.T., Sutin B., 1987, *ApJ*, 320, 803
 Draine B.T., Roberge W.G., Dalgarno A., 1983, *ApJ*, 264, 485
 Gibb E.L. et al., 2000, *ApJ*, 536, 347
 Gredel R., 1990, in Hartquist T.W., ed., *Molecular Astrophysics*. Cambridge Univ. Press, Cambridge, p. 305
 Gredel R., Lepp S., Dalgarno A., 1987, *ApJ*, 323, L137

- Jones A.P., Duley W.W., Williams D.A., 1990, QJRAS, 31, 567
 Jones A.P., Tielens A.G.G.M., Hollenbach D.J., McKee C.F., 1994, ApJ, 433, 797
 Jones A.P., Tielens A.G.G.M., Hollenbach D.J., 1996, ApJ, 469, 740
 Le Bourlot J., Pineau des Forêts G., Roueff E., Flower D.R., 1995, A&A, 302, 870
 Le Bourlot J., Pineau des Forêts G., Flower D.R., Cabrit S., 2002, MNRAS, 332, 985
 Li A., Draine B.T., 2001, ApJ, 554, 778
 Mathis J.S., Rumpl W., Nordsieck K.H., 1977, ApJ, 217, 425
 May P.W., Pineau des Forêts G., Flower D.R., Field D., Allan N.L., Purton J.A., 2000, MNRAS, 318, 809
 Omont A., 1986, A&A, 164, 159
 Pilipp W., Hartquist T.W., Havnes O., 1990, MNRAS, 243, 685
 Pineau des Forêts G., Flower D.R., Hartquist T.W., Dalgarno A., 1986, MNRAS, 220, 801
 Pineau des Forêts G., Flower D.R., Dalgarno A., 1988, MNRAS, 235, 621
 Prasad S.S., Tarafdar S.P., 1983, ApJ, 267, 603
 Savage B.D., Sembach K.R., 1996, ARA&A, 34, 279
 Sofia U.J., Meyer D.M., 2001, ApJ, 554, L221
 Sternberg A., Dalgarno A., Lepp S., 1987, ApJ, 320, 676
 Weingartner J.C., Draine B.T., 2001a, ApJS, 134, 263
 Weingartner J.C., Draine B.T., 2001b, ApJ, 548, 296

APPENDIX A:

In Table A1 we summarize the rate coefficients that were adopted when calculating the charge states of both large and small grains, as discussed in Section 2. The rates of detachment of electrons from neutral and negatively charged grains depend on the fraction of the H₂ fluorescence photons that are absorbed by PAH, and hence on the fractional abundance of PAH. Results are tabulated for $n_{\text{PAH}}/n_{\text{H}} = 10^{-6}$. When $n_{\text{PAH}}/n_{\text{H}} = 10^{-7}$ (or less), the values of γ for the third and fourth reactions in part (b) of Table A1 should be increased by 14 per cent.

Table A1. Rate coefficients adopted for reactions involving (a) PAH molecules ('very small grains') and (b) larger grains (Omont 1986; Pineau des Forêts et al. 1988; Weingartner & Draine 2001a). The rate coefficient is of the form $\gamma \exp(-\beta/T)(T/300)^\alpha(1 + 450\delta/T) \text{ cm}^3 \text{ s}^{-1}$, where T (K) is the effective temperature of the reaction [which allows for the ion-neutral drift speed, where appropriate; see Pineau des Forêts et al. (1986)] and $\delta = 1$ for a reaction between a positively and a negatively charged particle, $\delta = 0$ otherwise. For photoreactions, induced by fluorescence of H₂ following cosmic ray ionization of hydrogen, the rate (s^{-1}) is of the form $\gamma\zeta$, where ζ is the cosmic ray ionization rate. 'Section' refers to the section of the paper in which the reaction and its rate coefficient are considered.

Section	Reaction	γ	α	β
(a)				
2.1.1	$\text{PAH}^0 + \text{e} \rightarrow \text{PAH}^- + \text{phonon}$	1.00 (-07)	0.00	0.0
2.1.1	$\text{PAH}^+ + \text{e} \rightarrow \text{PAH}^0 + \text{phonon}$	3.30 (-06)	-0.50	0.0
2.1.2	$\text{PAH}^0 + \text{photon} \rightarrow \text{PAH}^+ + \text{e}$	2.00 (+04)	0.00	0.0
2.1.2	$\text{PAH}^- + \text{photon} \rightarrow \text{PAH}^0 + \text{e}$	2.00 (+04)	0.00	0.0
2.1.3	$\text{PAH}^- + \text{PAH}^+ \rightarrow \text{PAH}^0 + \text{PAH}^0$	3.00 (-09)	-0.50	0.0
2.1.3	$\text{PAH}^- + \text{H}^+ \rightarrow \text{PAH}^0 + \text{H}$	7.50 (-08)	-0.50	0.0
2.1.3	$\text{PAH}^- + \text{H}_3^+ \rightarrow \text{PAH}^0 + \text{H}_2 + \text{H}$	2.20 (-08)	-0.50	0.0
2.1.3	$\text{PAH}^- + \text{H}_3^+ \rightarrow \text{PAH}^0 + 3\text{H}$	2.20 (-08)	-0.50	0.0
2.1.3	$\text{PAH}^- + \text{He}^+ \rightarrow \text{PAH}^0 + \text{He}$	3.80 (-08)	-0.50	0.0
2.1.3	$\text{PAH}^- + \text{C}^+ \rightarrow \text{PAH}^0 + \text{C}$	2.20 (-08)	-0.50	0.0
2.1.3	$\text{PAH}^- + \text{H}_3\text{O}^+ \rightarrow \text{PAH}^0 + \text{H}_2\text{O} + \text{H}$	1.70 (-08)	-0.50	0.0
2.1.3	$\text{PAH}^- + \text{H}_3\text{S}^+ \rightarrow \text{PAH}^0 + \text{H}_2\text{S} + \text{H}$	1.30 (-08)	-0.50	0.0
2.1.3	$\text{PAH}^- + \text{NH}_4^+ \rightarrow \text{PAH}^0 + \text{NH}_3 + \text{H}$	1.80 (-08)	-0.50	0.0
2.1.3	$\text{PAH}^- + \text{HCO}^+ \rightarrow \text{PAH}^0 + \text{CO} + \text{H}$	1.40 (-08)	-0.50	0.0
2.1.3	$\text{PAH}^- + \text{HCS}^+ \rightarrow \text{PAH}^0 + \text{CS} + \text{H}$	1.10 (-08)	-0.50	0.0
2.1.3	$\text{PAH}^- + \text{Si}^+ \rightarrow \text{PAH}^0 + \text{Si}$	1.40 (-08)	-0.50	0.0
2.1.3	$\text{PAH}^- + \text{Fe}^+ \rightarrow \text{PAH}^0 + \text{Fe}$	1.00 (-08)	-0.50	0.0
2.1.3	$\text{PAH}^- + \text{S}^+ \rightarrow \text{PAH}^0 + \text{S}$	1.30 (-08)	-0.50	0.0
2.1.3	$\text{PAH}^0 + \text{H}^+ \rightarrow \text{PAH}^+ + \text{H}$	4.40 (-09)	0.00	0.0
2.1.3	$\text{PAH}^0 + \text{H}_3^+ \rightarrow \text{PAH}^+ + \text{H}_2 + \text{H}$	1.30 (-09)	0.00	0.0
2.1.3	$\text{PAH}^0 + \text{H}_3^+ \rightarrow \text{PAH}^+ + 3\text{H}$	1.30 (-09)	0.00	0.0
2.1.3	$\text{PAH}^0 + \text{He}^+ \rightarrow \text{PAH}^+ + \text{He}$	2.20 (-09)	0.00	0.0
2.1.3	$\text{PAH}^0 + \text{C}^+ \rightarrow \text{PAH}^+ + \text{C}$	1.30 (-09)	0.00	0.0
2.1.3	$\text{PAH}^0 + \text{H}_3\text{O}^+ \rightarrow \text{PAH}^+ + \text{H}_2\text{O} + \text{H}$	1.00 (-09)	0.00	0.0
2.1.3	$\text{PAH}^0 + \text{H}_3\text{S}^+ \rightarrow \text{PAH}^+ + \text{H}_2\text{S} + \text{H}$	7.40 (-10)	0.00	0.0
2.1.3	$\text{PAH}^0 + \text{NH}_4^+ \rightarrow \text{PAH}^+ + \text{NH}_3 + \text{H}$	1.00 (-09)	0.00	0.0
2.1.3	$\text{PAH}^0 + \text{HCO}^+ \rightarrow \text{PAH}^+ + \text{CO} + \text{H}$	8.20 (-10)	0.00	0.0
2.1.3	$\text{PAH}^0 + \text{HCS}^+ \rightarrow \text{PAH}^+ + \text{CS} + \text{H}$	6.50 (-10)	0.00	0.0
2.1.3	$\text{PAH}^0 + \text{Si}^+ \rightarrow \text{PAH}^+ + \text{Si}$	8.30 (-10)	0.00	0.0
2.1.3	$\text{PAH}^0 + \text{Fe}^+ \rightarrow \text{PAH}^+ + \text{Fe}$	5.90 (-10)	0.00	0.0
2.1.3	$\text{PAH}^0 + \text{S}^+ \rightarrow \text{PAH}^+ + \text{S}$	7.80 (-10)	0.00	0.0
2.1.4	$\text{PAH}^- + \text{H} \rightarrow \text{PAH}^0 + \text{CH} + \text{e}$	3.30 (-09)	0.00	5500
2.1.4	$\text{PAH}^- + \text{C} \rightarrow \text{PAH}^0 + \text{CH} + \text{e}$	9.60 (-10)	0.00	5500
2.1.4	$\text{PAH}^- + \text{CH} \rightarrow \text{PAH}^0 + \text{CH}_2 + \text{e}$	9.60 (-10)	0.00	5500
2.1.4	$\text{PAH}^- + \text{O} \rightarrow \text{PAH}^0 + \text{CO} + \text{e}$	8.30 (-10)	0.00	5500
2.1.4	$\text{PAH}^- + \text{OH} \rightarrow \text{PAH}^0 + \text{H}_2\text{O} + \text{e}$	8.30 (-10)	0.00	5500

Table A1 – *continued*

Section	Reaction	γ	α	β
(b)				
2.2.1	$g^0 + e \rightarrow g^- + \text{phonon}$	6.90 (–05)	0.50	0.0
2.2.1	$g^+ + e \rightarrow g^0 + \text{phonon}$	6.90 (–05)	0.50	0.0
2.2.2	$g^0 + \text{photon} \rightarrow g^+ + e$	0.55 (+08)	0.00	0.0
2.2.2	$g^- + \text{photon} \rightarrow g^0 + e$	0.36 (+09)	0.00	0.0
2.2.3	$g^0 + H^+ \rightarrow g^+ + H$	1.60 (–06)	0.50	0.0
2.2.3	$g^0 + H_3^+ \rightarrow g^+ + H_2 + H$	4.61 (–07)	0.50	0.0
2.2.3	$g^0 + H_3^+ \rightarrow g^+ + 3H$	4.61 (–07)	0.50	0.0
2.2.3	$g^0 + He^+ \rightarrow g^+ + He$	8.00 (–07)	0.50	0.0
2.2.3	$g^0 + C^+ \rightarrow g^+ + C$	4.61 (–07)	0.50	0.0
2.2.3	$g^0 + H_3O^+ \rightarrow g^+ + H_2O + H$	3.66 (–07)	0.50	0.0
2.2.3	$g^0 + H_3S^+ \rightarrow g^+ + H_2S + H$	2.70 (–07)	0.50	0.0
2.2.3	$g^0 + NH_4^+ \rightarrow g^+ + NH_3 + H$	3.76 (–07)	0.50	0.0
2.2.3	$g^0 + HCO^+ \rightarrow g^+ + CO + H$	2.96 (–07)	0.50	0.0
2.2.3	$g^0 + HCS^+ \rightarrow g^+ + CS + H$	2.38 (–07)	0.50	0.0
2.2.3	$g^0 + Si^+ \rightarrow g^+ + Si$	3.01 (–07)	0.50	0.0
2.2.3	$g^0 + Fe^+ \rightarrow g^+ + Fe$	2.13 (–07)	0.50	0.0
2.2.3	$g^0 + S^+ \rightarrow g^+ + S$	2.82 (–07)	0.50	0.0
2.2.4	$g^- + H^+ \rightarrow g^0 + H$	1.60 (–06)	0.50	0.0
2.2.4	$g^- + H_3^+ \rightarrow g^0 + H_2 + H$	4.61 (–07)	0.50	0.0
2.2.4	$g^- + H_3^+ \rightarrow g^0 + 3H$	4.61 (–07)	0.50	0.0
2.2.4	$g^- + He^+ \rightarrow g^0 + He$	8.00 (–07)	0.50	0.0
2.2.4	$g^- + C^+ \rightarrow g^0 + C$	4.61 (–07)	0.50	0.0
2.2.4	$g^- + H_3O^+ \rightarrow g^0 + H_2O + H$	3.66 (–07)	0.50	0.0
2.2.4	$g^- + H_3S^+ \rightarrow g^0 + H_2S + H$	2.70 (–07)	0.50	0.0
2.2.4	$g^- + NH_4^+ \rightarrow g^0 + NH_3 + H$	3.76 (–07)	0.50	0.0
2.2.4	$g^- + HCO^+ \rightarrow g^0 + CO + H$	2.96 (–07)	0.50	0.0
2.2.4	$g^- + HCS^+ \rightarrow g^0 + CS + H$	2.38 (–07)	0.50	0.0
2.2.4	$g^- + Si^+ \rightarrow g^0 + Si$	3.01 (–07)	0.50	0.0
2.2.4	$g^- + Fe^+ \rightarrow g^0 + Fe$	2.13 (–07)	0.50	0.0
2.2.4	$g^- + S^+ \rightarrow g^0 + S$	2.82 (–07)	0.50	0.0

This paper has been typeset from a Microsoft Word file prepared by the author.